Diurnal Variability of the Hydrologic Cycle and Radiative Fluxes: Comparisons between Observations and a GCM

XIN LIN, DAVID A. RANDALL, AND LAURA D. FOWLER

Department of Atmospheric Science, Colorado State University, Fort Collins, Colorado

(Manuscript received 11 October 1999, in final form 1 April 2000)

ABSTRACT

The simulated diurnal cycle is in many ways an ideal test bed for new physical parameterizations. The purpose of this paper is to compare observations from the Tropical Rainfall Measurement Mission, the Earth Radiation Budget Experiment, the International Satellite Cloud Climatology Project, the Clouds and the Earth's Radiant Energy System Experiment, and the Anglo-Brazilian Amazonian Climate Observation Study with the diurnal variability of the Amazonian hydrologic cycle and radiative energy budget as simulated by the Colorado State University general circulation model, and to evaluate improvements and deficiencies of the model physics. The model uses a prognostic cumulus kinetic energy (CKE) to relax the quasi-equilibrium closure of the Arakawa–Schubert cumulus parameterization. A parameter, α, is used to relate the CKE to the cumulus mass flux. This parameter is expected to vary with cloud depth, mean shear, and the level of convective activity, but up to now a single constant value for all cloud types has been used. The results of the present study show clearly that this approach cannot yield realistic simulations of both the diurnal cycle and the monthly mean climate state. Improved results are obtained using a version of the model in which α is permitted to vary with cloud depth.

1. Introduction

In the past few decades, tremendous effort has been expended to improve the parameterizations of moist processes, cloud–radiation interactions, and land surface processes used in general circulation models (GCMs). Evaluating these new parameterizations using available observations is a necessary and important step.

The simulated diurnal cycle is in many ways an ideal test bed for new physical parameterizations. Not only is the forcing of the diurnal cycle external to the climate system as conventionally defined, but also the nature of this forcing is very well understood and can be quantitatively specified with good accuracy. The diurnal cycle is of course periodic, so that compositing of observations and model results can be performed in a highly objective manner. In addition, the period of the diurnal cycle is short, so that a statistically significant diurnal signal can be extracted from a relatively brief simulation or a relatively brief observational record. Successful simulation of daily variability of the hydrologic cycle and radiative energy budget in a GCM represents an important test of the model's formulation (Slingo et al. 1987; Randall et al. 1991).

Corresponding author's address: Dr. Xin Lin, Department of Atmospheric Science, Colorado State University, Fort Collins, CO 80523-1371.
E-mail: lin@atmos.colostate.edu

Many tests of GCM output against observations focus on mean fields at monthly, seasonal, and annual timescales. There are apparent limitations to this approach. It is possible for GCMs to produce realistic climate states for the wrong reasons. Further comparisons of model results with data, now focusing on diurnal timescales, will enable us to better understand how the hydrologic cycle interacts with clouds and radiative fluxes. Monthly mean simulations can then be given more clear physical interpretations by revealing at what time during the day a model tends to behave well or badly.

To investigate the complexities of the diurnal variability produced by nature and GCMs, we would like to find a large area where 1) the causes of the diurnal variations of convection are relatively simple and easily understood, 2) the diurnal signal is strong and relatively uniform, 3) both convective and stratiform precipitation are copious, and 4) there are extensive observations of the hydrologic cycle and the radiative energy budget.

Numerous observations show that the diurnal variation of convection is generally stronger over land than over oceans, and that the strongest convection over the summer and tropical continents usually occurs in the late afternoon or early evening, due to the dominant influence of daytime boundary layer heating (e.g., Wallace 1975; Gray and Jacobson 1977; Short and Wallace 1980; Kousky 1980; Meisner and Arkin 1987; Liebmann and Gruber 1988; Duvel 1989; Hartmann et al. 1991; Hendon and Woodberry 1993; Bergman and Sal-

by 1996, 1997). As one of the largest landmasses in the Tropics, the Amazon Basin displays strong diurnal variations in convective activity during the Southern Hemisphere summer (Kousky 1980; Minnis and Harrison 1984; Silva Dias et al. 1987; Meisner and Arkin 1987; Liebmann and Gruber 1988; Hartmann et al. 1991; Kondragunta et al. 1993; Garreaud and Wallace 1997). Besides the strong diurnal signals, the Amazon Basin has the largest coverage of tropical rain forest, with abundant convective and stratiform precipitation in the southern summer. Furthermore, in addition to conventional observations, the Tropical Rainfall Measurement Mission (TRMM; Simpson et al. 1988) and the Large-scale Biosphere–Atmosphere Experiment in Amazonia (LBA) are providing extensive and unprecedented spaceborne and surface-based observations of the hydrologic cycle and radiative fluxes. In short, the Amazon region is an excellent site for investigating the diurnal variability of the hydrologic cycle and radiative energy budget over the tropical land surface, and for testing a model's parameterizations.

It is well known that strong surface heating due to incoming solar radiation drives the afternoon to early evening convection over summer continents. On the other hand, clouds and precipitation can sharply decrease the solar radiation reaching the surface, and strongly affect the phases and amplitudes of various surface fluxes, as well as the daytime maximum surface temperature (e.g., Karl and Steurer 1990; Karl et al. 1993; Bergman and Salby 1996, 1997; Dai et al. 1999a). Excluding work focused on the tides, there have been few published studies of GCM-simulated diurnal variability, let alone detailed comparisons against observations. Randall et al. (1991) were the first to address the seasonal-mean diurnal variability of the hydrologic cycle in a GCM, using an earlier version of the Colorado State University (CSU) GCM. Their results show fair agreement between the simulation and observations, with an afternoon precipitation maximum over land in the Tropics, and an early morning precipitation maximum over the ocean far from land. Chen et al. (1996) investigated the diurnal ranges of precipitation frequency, intensity and amount, as simulated by version 2 of the National Center for Atmospheric Research (NCAR) Community Climate Model, and noticed significant differences from observations. Dai et al. (1999b) examined the simulated diurnal cycle of precipitation over continental North America obtained with the NCAR regional climate model. They found that simulations with three different cumulus parameterizations all failed to capture the broad pattern of the diurnal cycle of precipitation, with overestimated precipitation frequency and underestimated precipitation intensity.

In this study we have used observations from TRMM, the Earth Radiation Budget Experiment (ERBE; Barkstrom 1984), the International Satellite Cloud Climatology Project (ISCCP; Rossow and Schiffer 1991), the Clouds and the Earth's Radiant Energy System Experiment (CERES; Wielicki and Barkstrom 1991), and the Anglo-Brazilian Amazonian Climate Observation Study (ABRACOS; Shuttleworth et al. 1991), and compared these data with simulations of the diurnal variability of the Amazonian hydrologic cycle and radiative energy budget. We are particularly interested in two sets of issues.

1) What are the seasonal mean diurnal variabilities of rainfall, radiative fluxes, and clouds over tropical summer continents? How do rainfall, radiative fluxes, and clouds interact with one another in nature? How long is the time lag between intense convective precipitation and the coldest outgoing infrared radiation?
2) Can the GCM capture these diurnal phenomena over the tropical continents? How sensitive is the GCM's diurnal variability to certain aspects of the physical parameterizations? What can we do to improve the GCM's simulations of convective diurnal variability?

Section 2 briefly discusses the observational data used in this study and how they have been analyzed. Section 3 introduces the CSU GCM, including its new physical parameterizations, and explains how the GCM output has been analyzed. Section 4 compares the simulated and observed tropospheric mean states. Section 5 compares the simulated and observed diurnal variability of precipitation, the top-of-atmosphere (TOA) and surface radiative fluxes, and high-cloud amount. As discussed below, the results show a sensitivity to the cumulus parameterization, such that with the current parameterization we can obtain a realistic simulation of the mean state, or a realistic simulation of the diurnal cycle, but not both. This unexpected result motivates us to alter the cumulus parameterization. Section 6 discusses the results of a simulation with the altered parameterization. Section 7 gives a summary and conclusions.

2. Observations

a. TRMM rainfall data

The TRMM satellite was launched in November 1997. Its purpose is to determine the temporal and spatial distributions of precipitation and latent heat in the Tropics and subtropics (Simpson et al. 1988; Kummerow et al. 1998). TRMM's orbit is circular, at an altitude of 350 km. The orbit has an inclination of 35° to the equator; the satellite visits each sampling area in low latitudes about once per day, but at a different local time every day. In this study we use data from the two primary rainfall instruments on TRMM, a multichannel passive microwave radiometer: the TRMM Microwave Imager (TMI; Kummerow et al. 1998), and a spaceborne quantitative precipitation radar (PR). The reason for using both TMI and PR rainfall retrievals is that they are based on different algorithms from different sensors, and examination of the consistency between these al-

gorithms can increase our confidence in the satellite-sampled rainfall observations. We have used the convective and stratiform rain flags provided with the TRMM PR data to separately analyze the convective and stratiform precipitation for comparison with the corresponding model results.

A simple accumulation method is used to calculate mean rain rates for each GCM grid cell. If the geolocation of a rainfall retrieval is within a 4° × 5° grid cell, then the rain rate and the number of occurrence are accumulated at 1-h intervals. Sensitivity tests indicate that there is little difference among simple averaging and various successive correction methods since the number of pixels is huge (Dr. S. Yang 1999, personal communication). Seasonal mean and seasonal diurnal rain rates in each grid cell are then obtained by dividing the accumulated rain rates by the total number of pixels. In a preliminary study, the sampling by the TRMM satellite was investigated using the CSU GCM. We found that in order to adequately sample diurnal variability at 1-h intervals, it is necessary to combine at least 3 months of TRMM pixel data on a 4° × 5° grid. In this study, we use TRMM data (version 4) from December 1997 to February 1998 and from December 1998 to February 1999.

b. ERBE, CERES, and ISCCP data

ERBE (Barkstrom 1984) was designed to improve our understanding of the TOA radiative balance of the climate system and to provide an accurate long-term dataset for evaluating climate simulations. The combination of the Earth Radiation Budget Satellite and one sun-synchronous satellite can sample all 24 h of local time in about 36 days at low latitudes (Brooks and Minnis 1984; Harrison et al. 1988; Hartmann et al. 1991). In this study, the monthly averaged hourly radiative fluxes from ERBE *S-9* were analyzed. The scanner data were averaged on a 2.5° × 2.5° grid over the globe. To ensure statistical significance of the data at diurnal timescales, and to avoid sampling problems, the first and second diurnal harmonics of longwave (LW) radiation data for the total scene (including clouds) were calculated using 4 yr of January data (1986–89).

The TRMM satellite carries a CERES instrument which provides ERBE-like measurements of radiative fluxes. The CERES instruments are improved models of the ERBE scanner instruments, which can also provide additional cloud and surface flux information (Wielicki and Barkstrom 1991). We have used CERES data for January and February 1998. We have compared the CERES longwave fluxes with those from ERBE and with GCM simulations.

ISCCP is designed to use satellite radiance measurements to infer the global distribution of cloud properties and their diurnal, seasonal, and interannual variations (Rossow and Schiffer 1991). The ISCCP D1 data provide 3-h global gridded cloud information with a spatial resolution of 2.5°. We used January high-cloud fraction data for 1986, 1987, 1990, 1991, 1992, and 1993. The high-cloud fraction is defined as the number of cloudy pixels with cloud top above 440 hPa divided by the total number of pixels. The first and second diurnal harmonics were calculated based on the 3-hourly data.

TABLE 1. Locations, measurement heights, and biome information of ABRACOS surface stations over the Amazon Basin.

Station	Symbol	Location	Biome	Measurement height
Manus	RD	2°57′S, 59°57′W	Forest	45 m
Maraba	RV	5°45′S, 49°10′W	Forest	52 m
Ji-Parana	RJ	10°05′S, 61°55′W	Forest	52 m
Manus	FD	2°19′S, 60°19′W	Pasture	Surface
Maraba	BS	5°10′S, 48°45′W	Pasture	6 m
Ji-Parana	NS	10°45′S, 62°22′W	Pasture	6 m
Manus	MS	3°6′S, 60°10′W	Urban	Surface

c. ABRACOS surface data

ABRACOS was designed to monitor the Amazonian climate and to provide data for the testing of GCMs (Shuttleworth et al. 1991). There were seven major surface stations. Table 1 shows the locations, biomes, and measurement heights of these stations. Three of them were inside primary forests, while the other three were inside cattle ranches covered mainly by pasture. The last one represents an urban climate.

Since the Amazon Basin is mostly covered by primary forest, in this study we use data from the three primary forest sites. These stations recorded hourly surface information of total incoming shortwave radiation, reflected shortwave radiation, net all-wave radiation, air temperature, wind direction and speed, rainfall, etc., from 1990 to 1996. December–January–February (DJF) mean diurnal variations of surface radiative fluxes and surface temperature were constructed by compositing these forest station data at 1-h intervals.

3. The CSU GCM

The CSU GCM is a finite-difference model that has been described, most recently, by Eitzen and Randall (1999). The diurnal variability of the hydrologic cycle, as simulated with an earlier version of the model, was discussed by Randall et al. (1991), but the model has been heavily revised since that time. Key changes since 1991 are that the current model uses the cumulus parameterization of Randall and Pan (1993) and Pan and Randall (1998), the stratiform cloud parameterization of Fowler et al. (1996), and the land surface parameterization of Sellers et al. (1996a,b).

As explained in sections 4 and 5, a particular aspect of the prognostic cumulus parameterization has turned out to be highly relevant to the present study, and so it is necessary to discuss the parameterization in a little more detail here. The parameterization uses a closure

based on a prognostic cumulus kinetic energy (CKE), so it can be called a prognostic cumulus parameterization. The prognostic CKE drastically simplifies the computations while at the same time eliminating some weaknesses of the original parameterization. This same cumulus parameterization is also being used by the GCM group at the University of California, Los Angeles, and by the Japan Meteorological Agency.

For each cloud type, Randall and Pan (1993) and Pan and Randall (1998) related the cloud-base cumulus mass flux, M_B to the CKE by a dimensional parameter, α:

$$M_B = \sqrt{(\mathrm{CKE})/\alpha}. \quad (1)$$

As emphasized by Randall and Pan (1993) and Pan and Randall (1998), there is absolutely no reason to expect that α is a constant. Equation (1) shows that, for a given value of the CKE, larger α means smaller M_B, and so smaller cumulus heating and drying rates. Pan and Randall (1998) found that as α increases, the simulated atmosphere tends to become cooler and more humid, with a smaller cumulus precipitation rate and a nearly compensating increase in the stratiform precipitation rate, as well as more shallow cumulus clouds. Pan and Randall's (1998) sensitivity tests indicate that larger values of α give more realistic monthly mean temperature in the tropical troposphere. Eitzen and Randall (1999) found that larger values of α lead to a considerable improvement in the simulated thermal structure and winds for the Asian summer monsoon. The earth's radiation budget was not well simulated in simulations performed with large values of α, although this result is obviously dependent on the cloudiness parameterization used.

Randall and Pan (1993) showed that the cumulus ''adjustment time'' defined by Arakawa–Schubert is closely related to the value of α; larger α corresponds to slower adjustment. In the context of the present study, this suggests that with a sufficiently large value of α the parameterized convection will not be able to respond to diurnal forcing as quickly as real convection does.

The current CSU GCM uses a single prescribed, constant value of α for all cloud types regardless of the meteorological environment of the convection. As discussed below, the results of the current study show that this approach is unsatisfactory.

In sections 4 and 5, we examine the simulated mean states and diurnal variability of the Amazonian hydrologic cycle and radiative energy budget in tests using two different values of α: 10^8 and 10^9 m^4 kg^{-1}. These values are suggested by the results of numerical experiments with a cloud-resolving model by Xu and Arakawa (1992). We have performed an Atmospheric Model Intercomparison Project–style (Gates 1992) simulation with each of these two values of α; in the following discussion, we refer to these two runs as Alpha8 and Alpha9. Observed monthly mean sea surface temperature and sea ice distributions provide realistic forcings for the model. Each run consists of a 10-yr simulation from January 1979 to December 1988. The runs were started on 31 October 1978 to allow the model to spin up. Data over the Amazon area have been saved at 1-h intervals. The first and second diurnal harmonics have been calculated, as in Randall et al. (1991), based on these 10-yr DJF ensemble means.

4. Simulations of monthly means

Pan and Randall (1998) and Eitzen and Randall (1999) have already discussed the sensitivity of the simulated mean structure of the troposphere to the prescribed value of α. The results of our simulations are consistent with their findings. Briefly, Alpha8 produces a warmer-than-observed tropical troposphere between 2 and 15 km, with a maximum error of 6 K at 12 km. The simulated troposphere is cooler than observed below 2 km. Alpha9 produces a generally cooler troposphere, and the warmer-than-observed maximum in tropical upper troposphere is greatly reduced (by about 4 K). The zonal mean temperature structure of Alpha9 is in much better agreement with observations than that of Alpha8 in the mid- and upper troposphere, but slightly worse at low levels. In both runs, the simulated lower tropical troposphere is generally drier than the observed. However, Alpha9 tends to be more realistic and has a smaller dry bias than Alpha8. The simulated wind field is also more realistic in Alpha9 than in Alpha8. *In summary, Alpha9 produces a more realistic mean state of the tropical troposphere.* For further discussion, see Pan and Randall (1998) and Eitzen and Randall (1999).

Figure 1 compares the January-mean outgoing longwave radiation (OLR) from Alpha8 and Alpha9 against ERBE observations. A low bias exists in both simulations; the global mean OLR values from Alpha8 and Alpha9 underestimate the ERBE data by 12 and 15 W m^{-2}, respectively. The low bias is mainly concentrated in the Tropics and subtropics, as well as the midlatitudes of the Southern Hemisphere. The simulated clear-sky OLR maps also exhibit a cold bias in low latitudes and summer hemisphere midlatitudes (not shown). The global means of the clear-sky OLR from Alpha8 and Alpha9 underestimate the ERBE data by 5 and 8 W m^{-2}, respectively (not shown). We conclude that excessive cloudiness and excessive water vapor contribute about equally to the underestimated OLR in the two simulations. Alpha8 appears to do a better job than Alpha9 in the Tropics and subtropics, since the low-α run tends to produce a drier atmosphere with a smaller shallow cumulus population in the Tropics. In the extratropics, the two model runs yield similar zonal-mean OLR values.

Although the OLR patterns are similar between the simulations and the ERBE data, there are some significant differences. 1) The intertropical convergence zone (ITCZ) band over the Pacific and Indian Oceans is much stronger and more extensive than observed in both simulations, indicating that too many high clouds are sim-

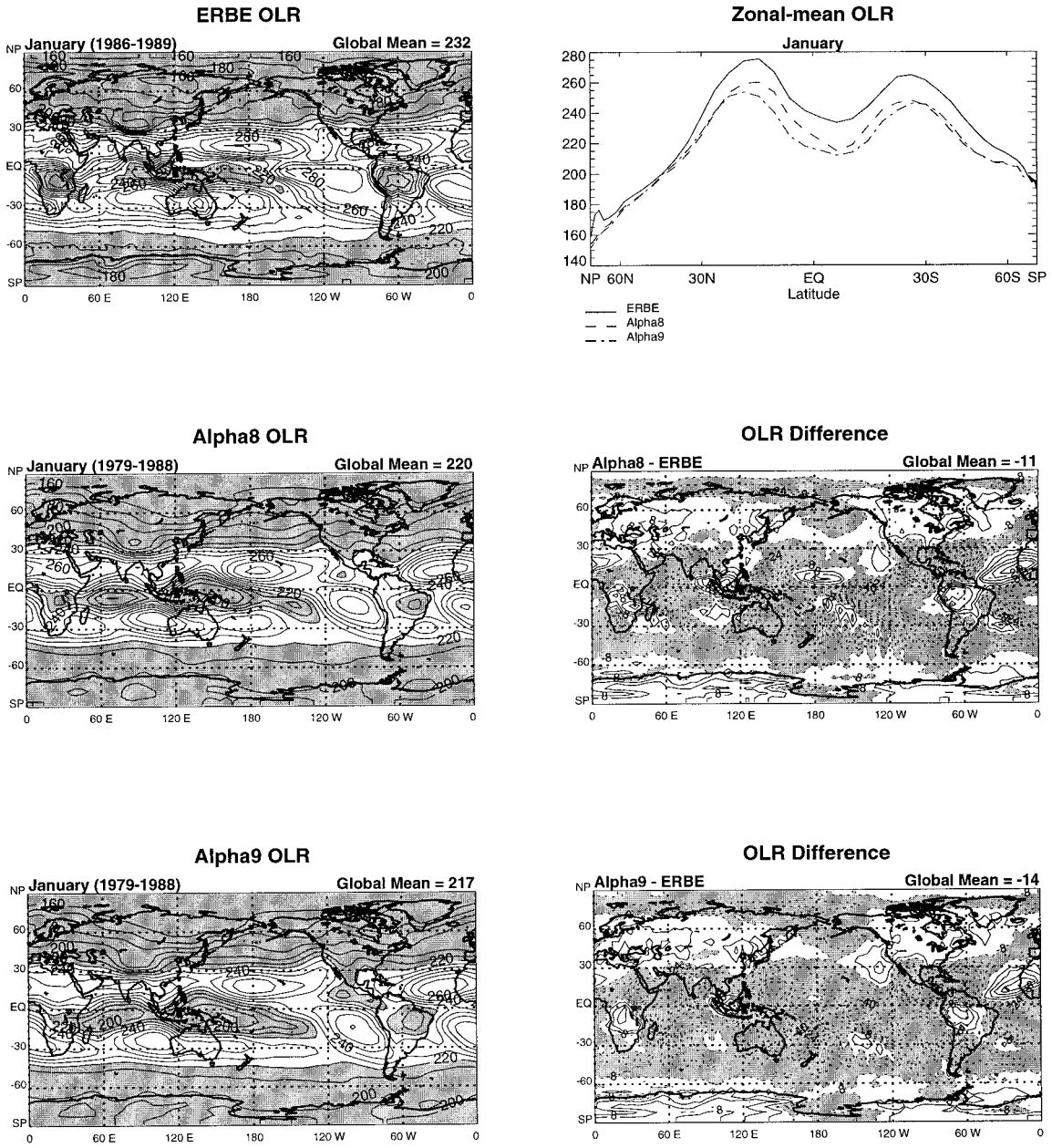

FIG. 1. Observed and simulated Jan-mean OLR and their differences: (a) ERBE OLR, (b) Alpha8 OLR, (c) Alpha9 OLR, (d) Zonal mean of Jan OLR, (e) Alpha8-ERBE, and (f) Alpha9-ERBE. The contour intervals for January-mean OLRs and their differences are 10 and 8 W m^{-2}, respectively. The OLR values below 220 W m^{-2} and the difference values below -8 W m^{-2} are lightly shaded.

ulated over the tropical oceans. 2) Over the tropical continents where deep convection usually dominates, such as the Amazon region, the Congo basin, and the Maritime Continent, the simulated OLR is greater than that observed, suggesting that there are not enough simulated high clouds.

Figure 2 compares the DJF total precipitation from Alpha8 and Alpha9 with data from the Global Precipitation Climatology Project (GPCP; Xie and Arkin 1996) combined DJF precipitation (Huffman et al. 1997), as well as TRMM rainfall retrievals from both TMI and PR. Although different years of data were used to construct the DJF precipitation ensembles, the two simulations and three sets of observations all exhibit similar large-scale distributions of total precipitation in the Tropics and subtropics (remember that TMI and PR only have data between $-40°$ and 40°). A strong ITCZ along the equator, extending from tropical Africa to the western Pacific, is observed and also well captured by the GCM simulations, although Al-

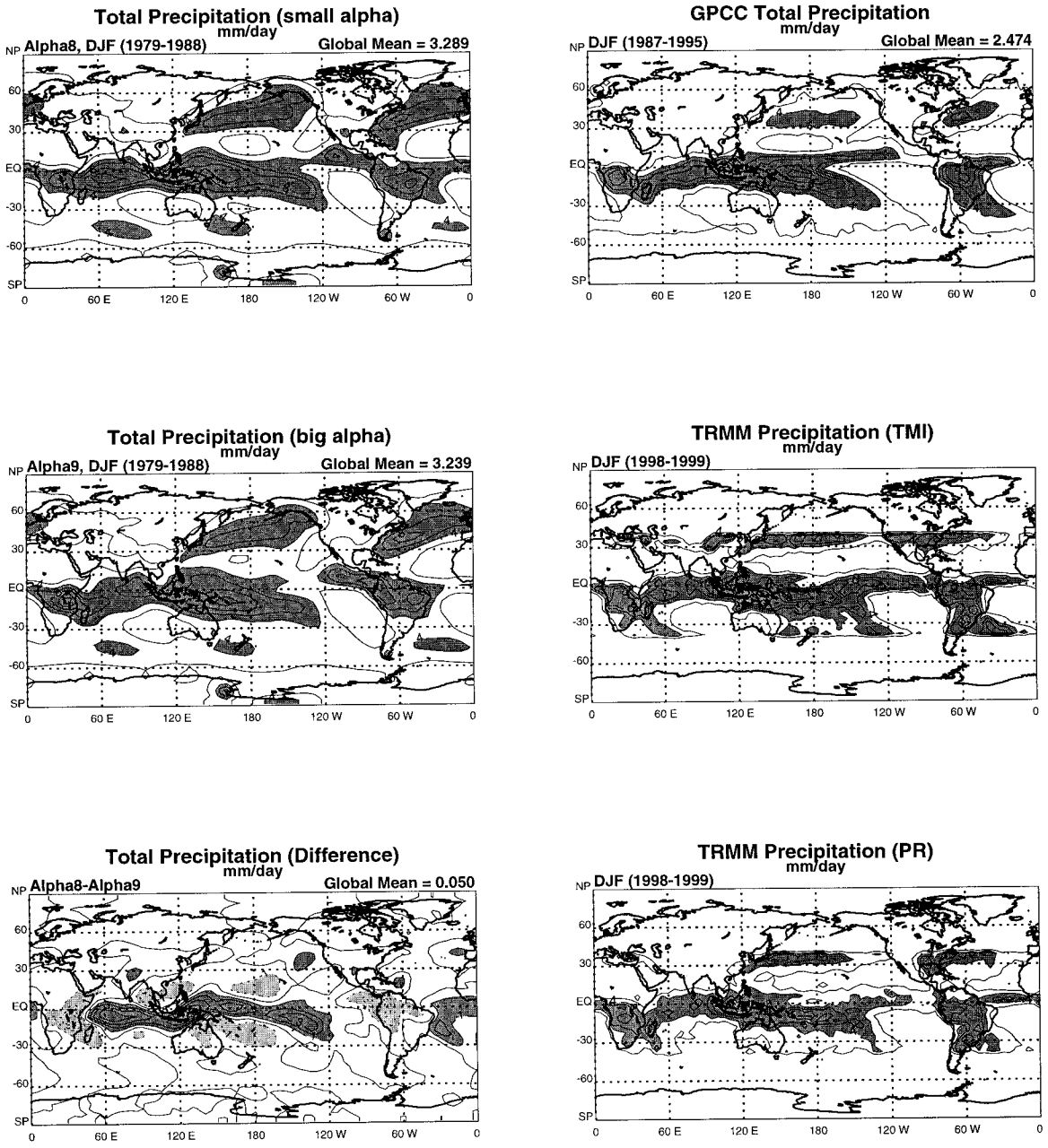

FIG. 2. The simulated and observed DJF mean precipitation distributions and their differences. (The units are mm day^{-1} and the contour intervals are 2 mm day^{-1}.) The rainfall values above 4 mm day^{-1} are darkly shaded. The rainfall difference values above 1 mm day^{-1} and below -1 mm day^{-1} are darkly and lightly shaded, respectively.

TABLE 2. Simulated and observed area mean rainfall rates between 40°S and 40°N.

	Alpha8	Alpha9	GPCC	TRMM TMI	TRMM PR
Rainfall (mm day^{-1})	3.665	3.585	3.110	3.561	3.211

pha8 shows a stronger ITCZ than Alpha9 along the equatorial Indian and Pacific Oceans. The area-mean rainfall rates between $-40°$ and 40° are 3.67, 3.59, 3.11, 3.56, and 3.21 mm day^{-1} for Alpha8, Alpha9, GPCC, TMI, and PR, respectively (see Table 2). Alpha8, Alpha9, and GPCP show that the equatorial ITCZ band in the Pacific Ocean is oriented from northwest to southeast across the western and central Pacific, where TRMM data show the ITCZ band along the equator. This is probably due to the use of only

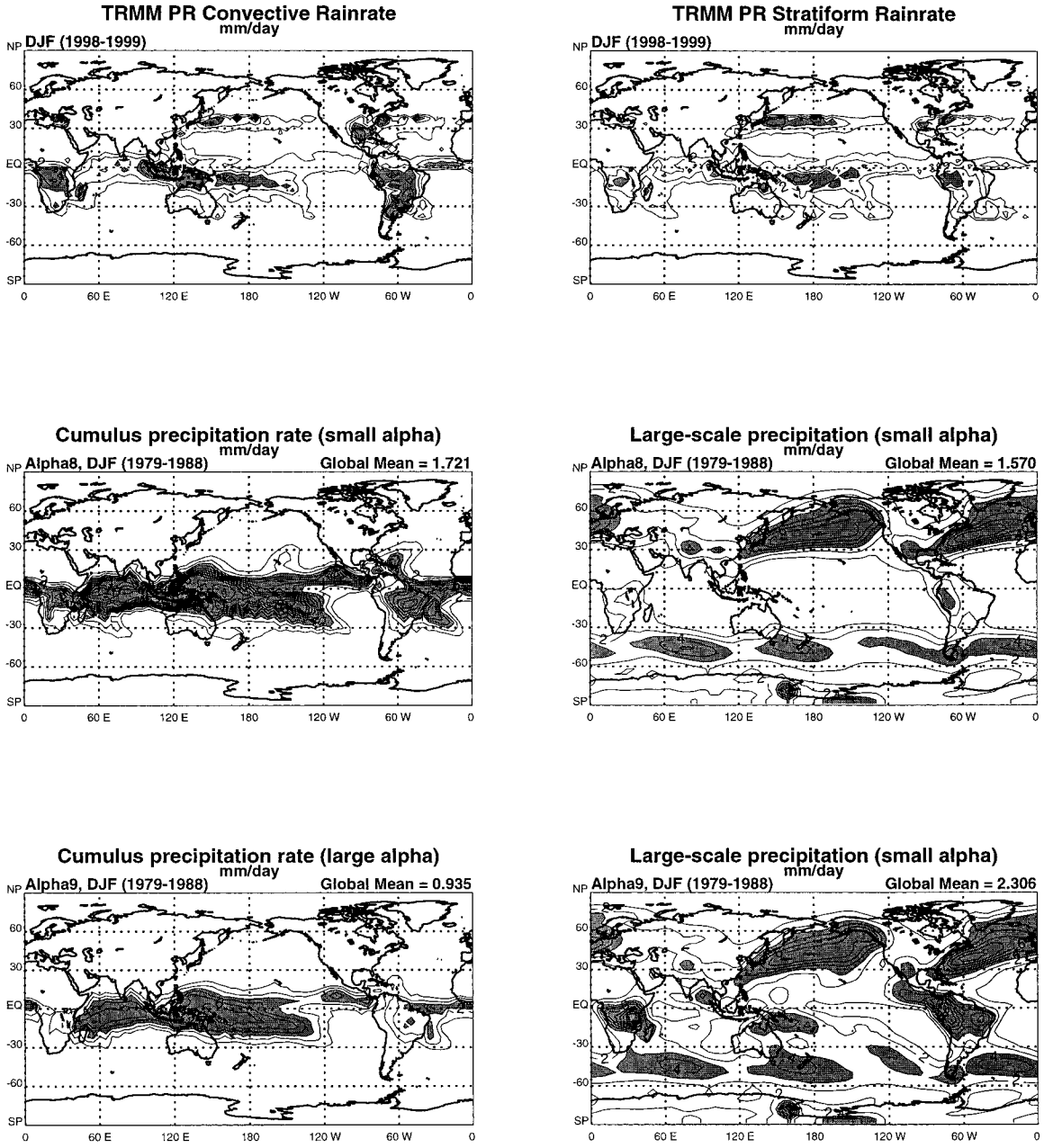

FIG. 3. The simulated and observed DJF convective and stratiform precipitation. (The units are mm day^{-1} and the contour intervals are 1 mm day^{-1}.) The values above 3 mm day^{-1} are darkly shaded.

two years of seasonal TRMM data (a total of 6 months) to construct the rainfall ensembles, and to the large interannual variability.[1] Rainfall rates from TRMM PR are generally smaller over the tropical oceans than those from TRMM TMI, especially over the eastern Pacific. In mid- and high latitudes, Alpha8 and Alpha9 both capture the broad features of the wintertime storm tracks in the North Pacific and Atlantic Oceans, with larger-than-GPCP but similar-to-TRMM rainfall rates. The simulated storm track in the Pacific Ocean is oriented from southwest to northeast, while the GPCP-observed one is more zonally oriented. Both simulations produce a somewhat realistic precipitation maximum over the Amazon Basin.

Figure 3 shows the observed and simulated DJF convective and stratiform precipitation. The observed convective rainfall pattern is similar to that of the simulated

[1] In particular 1998 was a strong El Niño year.

total precipitation, but so is the observed pattern of the stratiform rainfall. The observed convective rainfall rate over the tropical summer continents has amplitudes similar to those observed over the Maritime Continent and the equatorial western Pacific. There is weak convective precipitation associated with the winter hemisphere storm tracks in the midlatitudes. Both Alpha8 and Alpha9 have stronger-than-PR convective precipitation in the Tropics, but little convective precipitation in midlatitudes. The simulated convective rain rates over the tropical summer continents are much weaker than their counterparts over the equatorial tropical oceans. The observed stratiform precipitation is generally stronger than the observed convective rainfall rate in midlatitudes, but weaker in the Tropics, although their distribution patterns are similar. One interesting feature is that over the central equatorial Pacific (between 160°E and 150°W), the convective and stratiform precipitation rates are similar in magnitude. Both GCM runs show strong stratiform precipitation in the midlatitude storm track regions. Alpha8 tends to produce realistic stratiform rainfall rates over the tropical summer continents, but unrealistically weak stratiform rainfall rates over the tropical oceans. Alpha9 shows mostly stronger-than-Alpha8 stratiform precipitation, especially over the tropical summer continents.

In summary, Alpha9 tends to produce a better simulation of the large-scale monthly mean dynamic and thermodynamic structure in the tropical troposphere, while Alpha8 tends to simulate more realistic TOA radiative fluxes. Comparisons of observed and simulated long-term mean DJF precipitation indicate that 1) simulations with various values of α can capture most of the observed large-scale features of the total precipitation distribution; 2) the observed convective and stratiform precipitation have similar distribution patterns, although the convective precipitation dominates in the Tropics, while the stratiform precipitation dominates in midlatitudes. The simulated convective and stratiform precipitation have different distributions, with the simulated convective rainfall concentrated in the Tropics, and the simulated stratiform rainfall dominating in midlatitudes.

5. Diurnal cycle

a. Precipitation

Figure 4 shows global maps of the observed and simulated first diurnal harmonic of the DJF total precipitation rate. It is apparent that the satellite-sampled diurnal signals are generally stronger over the tropical continents such as the Amazon Basin and tropical Africa. The maxima over the tropical summer continents tend to occur between late afternoon and early evening, and the zonal-mean amplitude is about 3–5 mm day^{-1}. Over the tropical oceans, where deep convection usually dominates, the average amplitude of the first diurnal harmonic is about 1–2 mm day^{-1}, and the maxima tend to occur in the morning. This is well known from previous studies (e.g., Gray and Jacobsen 1977). Over other parts of the low-latitude oceans, especially the subtropics and the eastern parts of the tropical oceans, the amplitudes of the first diurnal harmonic are generally very small, and the phases are hard to distinguish. Alpha8 shows phases similar to those observed, with an afternoon to early evening maximum over the tropical continents, and an early morning precipitation maximum over the tropical oceans where convection dominates. However, the simulated amplitude of the first diurnal harmonic is smaller than observed over the tropical oceans. *Alpha9 produces a strikingly different and much less realistic phase pattern over the tropical summer continents, with a near-midnight maximum over the Amazon Basin, and an early morning maximum over tropical Africa.* The simulated amplitudes over both tropical continents and tropical oceans are smaller than observed.

Figure 5 examines the first diurnal harmonic of the total precipitation over South America derived from Alpha8, Alpha9, TMI, and PR. Observations show that there are variations of the phase and amplitude across the Amazon, but the overall patterns are similar between TMI and PR. The TMI data show an evening maximum (2000 LST) over the central and southern parts of the Amazon Basin, and a generally late night maximum over the northern part of the Amazon and northeast coast. The PR data indicate evening maxima (2000 LST) over the southern portion of the Amazon, and afternoon maxima (1600 LST) over the central and northern parts of the Amazon. The phases observed using TMI and PR are sightly different over the central and northern Amazon, presumably due to both the differences between the respective retrieval algorithms and sampling difference resulting from different swath widths. The Alpha8 simulation captures most of the features observed by TRMM, with an evening maximum over the northern and southern parts of the Amazon, and a late afternoon maximum over the central Amazon. The amplitude is slightly smaller than observed. The corresponding results from Alpha9 are considerably different from both the observations and Alpha8, and systematically exhibit a dominance of nocturnal and early morning maxima over the Amazon. This is associated with unrealistically strong stratiform precipitation over the tropical summer continents in Alpha9. The amplitude of the first diurnal harmonic in Alpha9 is generally much smaller than observed.

Figure 6 shows the second diurnal harmonic of the total precipitation from Alpha8, Alpha9, TMI, and PR. Both TMI and PR show that the observed semidiurnal mode peaks at 1400–1500 LST (and 0200–0300 LST). The amplitude is relatively strong, and reaches about 2–3 mm day^{-1}. This is different from the results of Meisner and Arkin (1987) in which the first harmonic of cold-cloud-derived precipitation was found to explain

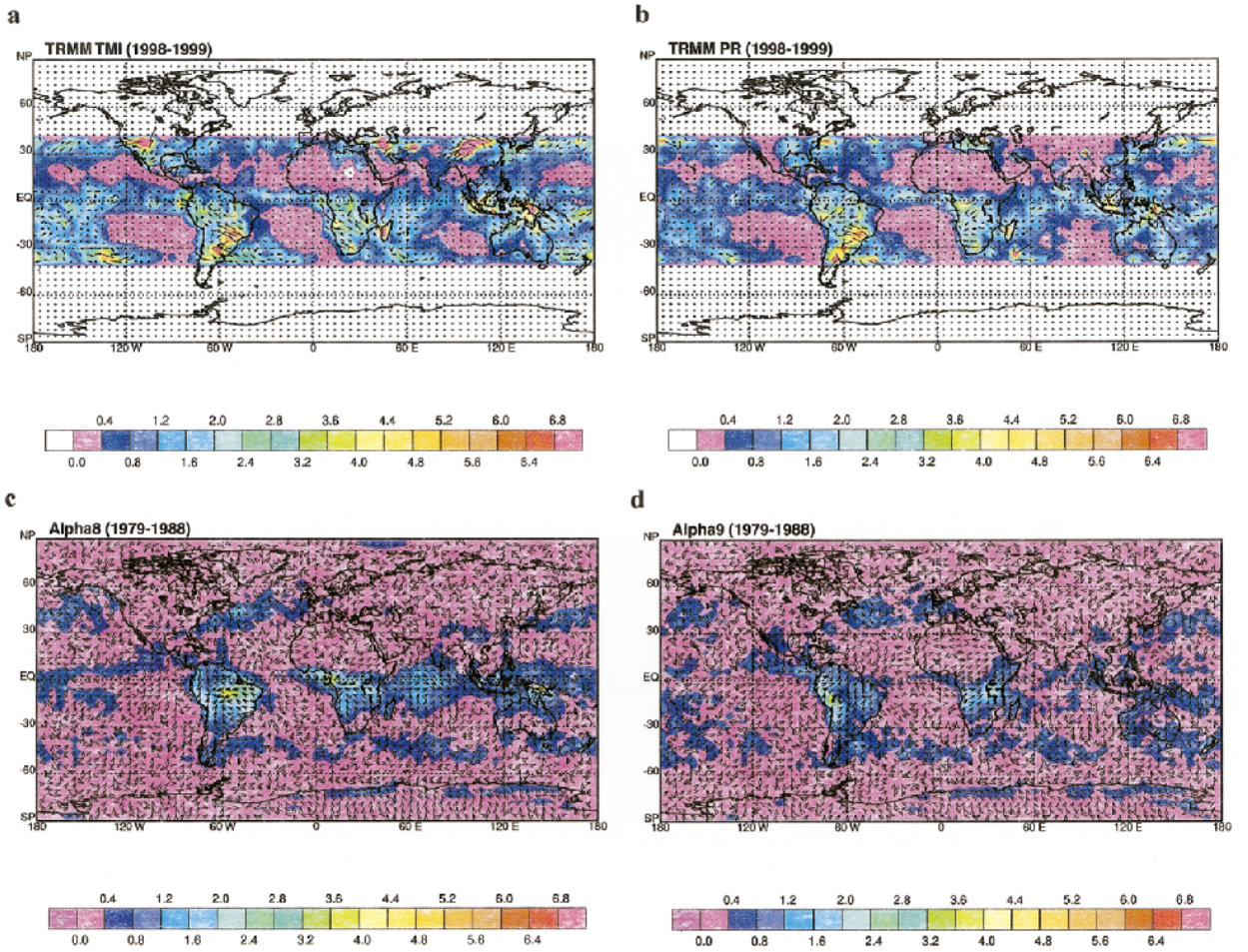

FIG. 4. Observed and simulated global maps of the first diurnal harmonic of DJF total precipitation rates: (a) TRMM TMI, (b) TRMM PR, (c) Alpha8, and (d) Alpha9. (The units are mm day^{-1} and the contour intervals are 0.4 mm day^{-1}.) Arrows pointing upward indicate maxima at local midnight, those pointing to the right indicate maxima at 0600 LST, etc. Note that TRMM TMI and PR data only have values between $-40°$ and 40°.

most of the variance. The discrepancy stems from the time lag between the heaviest surface precipitation and the coldest cloud tops, as will be discussed later. Both Alpha8 and Alpha9 have weaker-than-observed semidiurnal modes, with average amplitudes of about 1 mm day^{-1} or less. The semidiurnal mode in Alpha8 tends to show a maximum at 0300 LST (and 1500 LST), while in Alpha9 the maximum tends to occur at 0600 LST (and 1800 LST).

Figure 7 shows the composited diurnal time series of DJF total, convective, and stratiform rain rates over the Amazon from Alpha8, Alpha9, TMI, and PR. Both TMI and PR data (Fig. 7a) indicate a total precipitation minimum in the morning between 0900 and 1000 LST. Rain rates increase dramatically after 1100 LST, and reach peaks at 1500 LST for PR, and 1600 LST for TMI. The timing of maximum rain rate is consistent with observations from surface stations over the Amazon and other tropical and midlatitude continents (e.g., Wallace 1975; Kousky 1980; Liebmann et al. 1998; Dai et al. 1999a). Both the TMI and PR retrievals also indicate a second peak at about 1800 LST. Rainfall retrievals from PR are generally lower than TMI retrievals in the evening and nighttime, and higher during morning and early afternoon, presumably due to different retrieval algorithms. The mean Amazonian rain rates from TMI and PR are 7.4 and 7.1 mm day^{-1}, respectively. The Alpha8 rainfall time series shows a morning minimum at about 0900–1000 LST, similar to that observed, and an early evening peak at 1800 LST, about 2–3 h later than observed. The mean rain rate is 6.7 mm day^{-1}, and the diurnal range is smaller than observed. The diurnal variation of precipitation in Alpha9 is quite different from the observations and from Alpha8. The change of α from 10^8 to 10^9 m^{-4} kg^{-1} disrupts the diurnal variation of precipitation over the summer continents. The Alpha9 curve indicates a very weak double peak structure: the major and broader peak is at 0400 LST and the second peak at 1900 LST. The mean rainfall rate for Alpha9 is 7.7 mm day^{-1}.

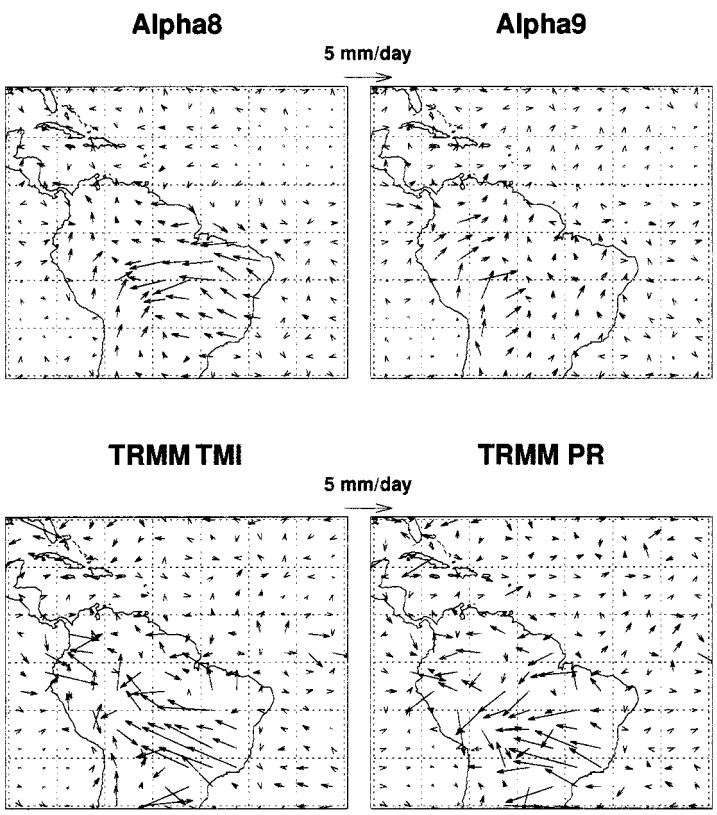

FIG. 5. Observed and simulated first diurnal harmonic of DJF total precipitation rates from Alpha8, Alpha9, TRMM TMI, and TRMM PR.

The observed diurnal cycle of the convective rain rate (Fig. 7b) is similar to that of the observed total rain rate, with a minimum (1 mm day^{-1}) between 0900 and 1000 LST, and a maximum (8 mm day^{-1}) between 1400 and 1600 LST. The Alpha8 convective rain rate shows a minimum (2.7 mm day^{-1}) at 0900 LST, and a maximum (8.2 mm day^{-1}) at 1800 LST. The diurnal range is similar to that observed, but the maximum rain rate lags the observed rate by 2–3 h, as for the total precipitation. The Alpha8 convective rain rate is generally larger than observed, except during the afternoon when convection rapidly develops. The Alpha9 convective rain rate shows a minimum (1.6 mm day^{-1}) between 0900 and 1100 LST, and a maximum (3.2 mm day^{-1}) at 1900 LST. Its maximum rain rate lags the observations by 3–4 h, and the diurnal range is much smaller.

The observed stratiform precipitation (Fig. 7c) over the Amazon shows a double peak structure with similar amplitudes. The broad peak between 1200 and 1600 LST corresponds to the period of relatively strong convective rainfall, and the ratio of convective to stratiform precipitation rates is about 2:1, suggesting that abundant stratiform clouds coexist with vigorous, deep cumuli in the afternoon over the tropical summer continents. This seems to contradict the conventional idea (e.g., Houze 1982; Rutledge and Houze 1987; Houze 1989) that the maximum stratiform precipitation rate tends to occur a few hours later than the maximum convective precipitation rate. Another peak occurs in the early morning between 0100 and 0400 LST, where the ratio of convective to stratiform rates is about 1:1, indicating the important role played by redeveloping stratiform clouds at night. Both simulations capture the early morning stratiform rainfall peak, although they again lag the observations by about 2–4 h. Alpha8 and Alpha9 show similar diurnal ranges, with a single maximum in the early morning between 0400 and 0600 LST, and a single minimum in the afternoon between 1400 and 1700 LST. Except for the afternoon stratiform rainfall peak, the stratiform rain rate from Alpha8 is very similar to that observed from TRMM. The Alpha9 stratiform rain rate is about 3 mm day^{-1} higher than that from Alpha8

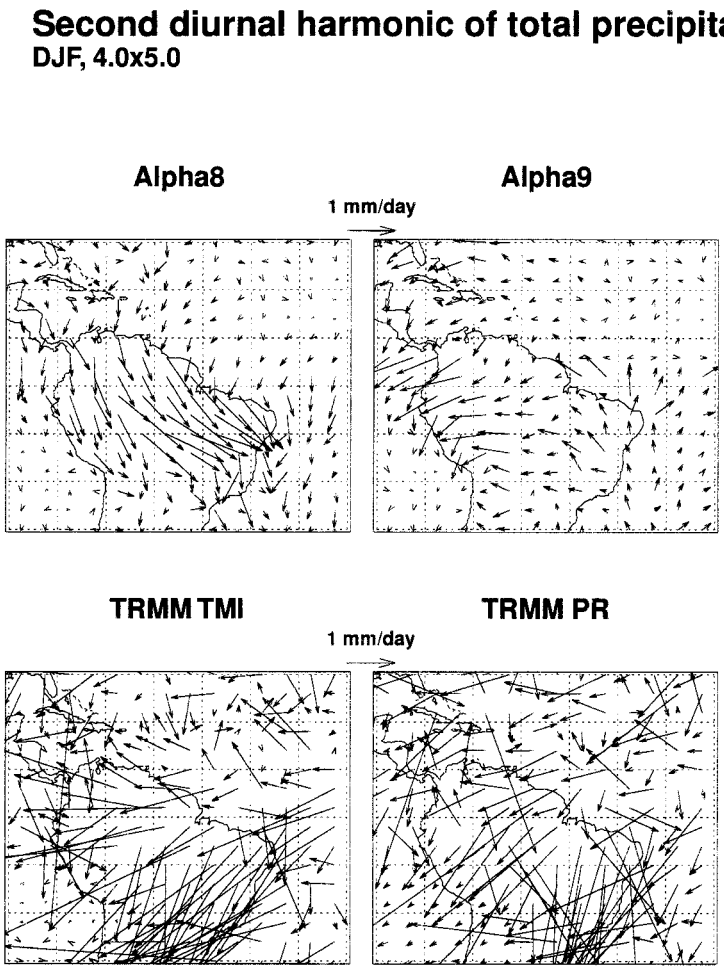

FIG. 6. Observed and simulated second diurnal harmonic of DJF total precipitation rates from Alpha8, Alpha9, TRMM TMI, and TRMM PR.

throughout the day and tends to lag the observations more.

These results demonstrate that, although the long-term seasonal-mean total precipitation simulated by the GCM is similar to that observed, the diurnal variations of precipitation, including convective and stratiform rainfall, are quite different from those observed especially for Alpha9. This illustrates that examining GCMs at the diurnal timescales will help us better identify various deficiencies in the model physics. In summary, the diurnal variation of rainfall over the Amazon shows several major similarities and differences between model runs and observations.

1) The diurnal variations of observed convective and stratiform precipitation are quite different over the tropical summer continents. In general, the convective rainfall tends to have a maximum in the afternoon, while the stratiform rainfall tends to have a maximum in the early morning. *The CSU GCM can capture these basic features.* As α increases, the GCM tends to produce smaller convective rain rates and larger stratiform rain rates. Such a change will definitely affect the diurnal variation of simulated total precipitation. It has therefore been helpful to use both the observed convective and stratiform rain rates to evaluate and constrain the cumulus and stratiform cloud parameterizations.
2) *Heavy stratiform precipitation is also observed in the afternoon, within the same period as heavier convective precipitation.* The simulations, in contrast, indicate only stratiform rainfall minima in the afternoon. It is of course possible that the cloud type classification schemes used with the PR data have some aliasing problems and need further improvement. However, if the PR-derived phenomenon is real, which is likely as pointed out by Houze (1997), then the relationship between convective and stratiform rainfall needs to be reconsidered, and the parameterization of stratiform rainfall in the GCM needs to be improved.
3) The diurnal ranges of the total rainfall rates from Alpha8 and Alpha9 are smaller than observed, but

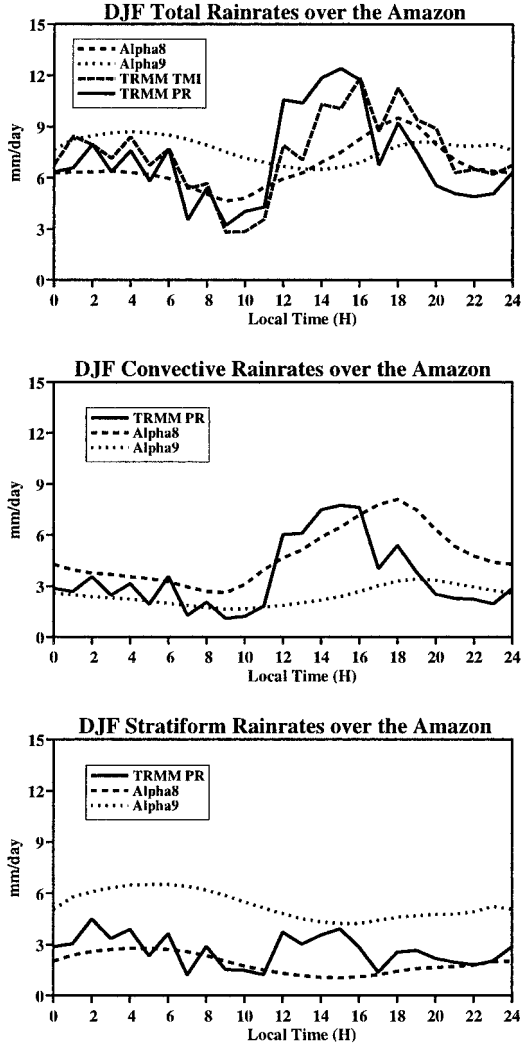

FIG. 7. Diurnal time series of observed and simulated DJF total, convective, and stratiform precipitation rates over the Amazon (mm day^{-1}).

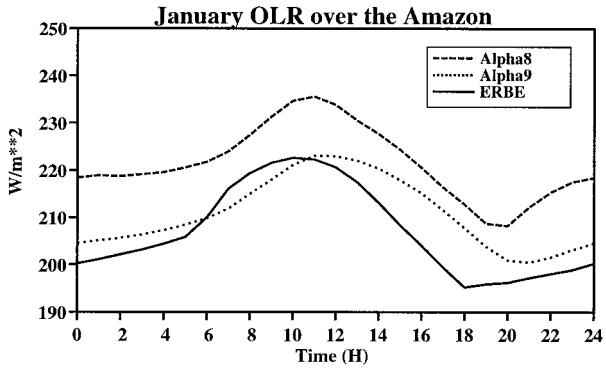

FIG. 8. Mean diurnal cycle of observed and simulated Jan OLR over the Amazon (W m^{-2}).

the daily mean values are close to the observations. As α increases, the diurnal range of precipitation, especially the convective precipitation, becomes unrealistically small. In addition, the maximum convective rainfall rate from Alpha8 lags observations by 2–3 h, while the Alpha9 maximum convective rainfall rate lags observations by 3–4 h. This suggests that, in *response to daytime surface heating, convection over the tropical continents develops much more slowly and weakly in the Alpha9 run than in the real world.* This is probably the reason why the simulated second diurnal harmonic of the total precipitation is so weak in the Alpha9 simulation, compared to observations. We return to this point later.

b. OLR

Figure 8 shows mean diurnal cycle of the summertime OLR over the Amazon from Alpha8, Alpha9, and ERBE data. The ERBE indicate an OLR maximum between 1000 and 1100 LST, and a minimum at 1800 LST, consistent with those observed in previous studies (e.g., Meisner and Arkin 1987; Harrison et al. 1988; Hartmann et al. 1991; Kondragunta et al. 1993). By comparing this result again the TRMM TMI and PR rainfall time series (Fig. 7), we can infer that on the average 0900–1100 LST is the time when the Amazon region is dominated by shallow nonprecipitating clouds and clear skies. More and deeper precipitating clouds (including both convective and stratiform clouds) start to develop rapidly after 1100 LST. The heaviest precipitation, presumably mostly from vigorous deep cumuli, occurs between 1500 and 1600 LST, but high-level clouds continue to grow by extending to cover a larger area and/or by growing deeper, and peak at 1800 LST. *The time lag between the maximum rainfall rate and the coldest cloud top over the Amazon is about 2–3 h.* From 1800 to 0500 LST the next morning, the OLR increases at a slow but steady pace (from 195 to 205 W m^{-2} over 11 h), suggesting that high-level clouds slowly dissipate during the night. Mid- and low-level clouds cover large areas, and many may persist until dawn. The observed sequence of nighttime cloud types is similar to those inferred by Hartmann et al. (1991) and Garreaud and Wallace (1997). Both TMI and PR data appear to show a minor but broad peak between 0100 and 0500 LST. By examining the fractions of convective and stratiform precipitation rates (1:1) from the TRMM PR data (Fig. 8), we can infer that there are lots of stratiform clouds coexisting with the cumuli during the night. Strong radiative cooling at the tops of these clouds tends to destabilize the mid- and upper troposphere (Randall et al. 1991), thus producing a weak but broad rainfall peak in the early morning, after a few hours of adjustment. After 0500 LST, the clouds dissipate rapidly, starting from the upper levels. The OLR increases dramatically and peaks between 1000 and 1100 LST.

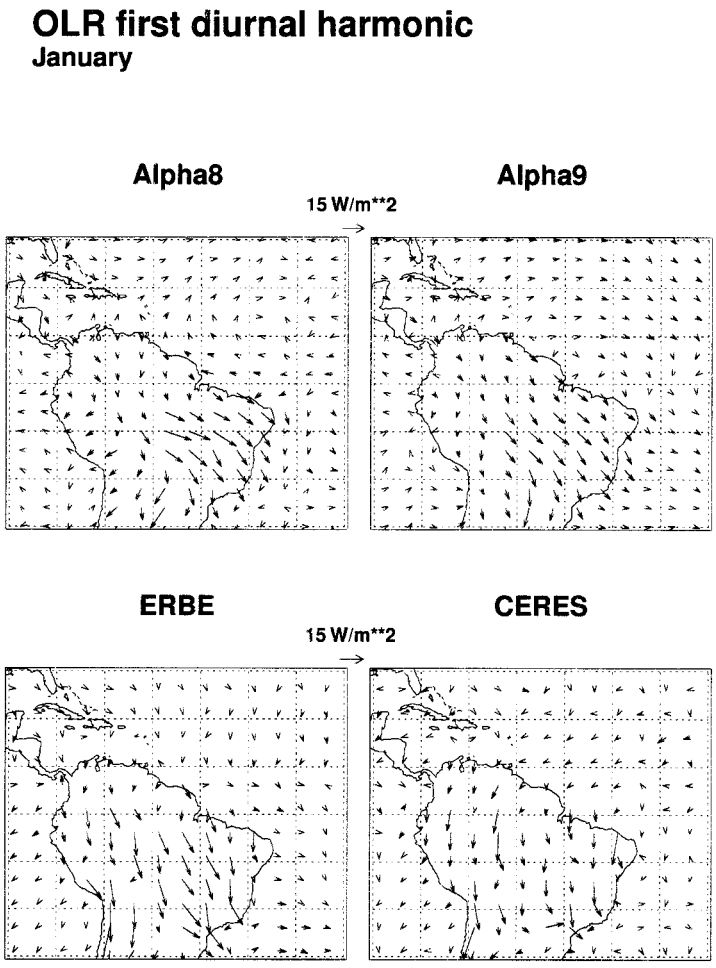

FIG. 9. Observed and simulated first diurnal harmonic of Jan OLR from Alpha8, Alpha9, and ERBE and CERES data.

Alpha8 produces an OLR maximum at 1100 and a minimum at 2000 LST. It overestimates the ERBE data by about 15–20 W m^{-2}, primarily because the Alpha8 atmosphere is too dry and has fewer clouds than observed over the tropical summer continents. This difference is especially serious during the night, but slightly better in the morning between 0600 and 1000 LST, suggesting that high-level clouds, which are dominant during the night, are not well represented in Alpha8. The time lag between the heaviest precipitation and the coldest cloud top is 2 h, similar to observations. The Alpha9 time series is more comparable with the ERBE data in terms of the OLR, although it still overestimates the ERBE data by 5–10 W m^{-2} in the afternoon and at night. The Alpha9 OLR shows a maximum at 1100 and a minimum at 2100 LST. Generally speaking, both simulations appear to respond sluggishly to the rapidly varying diurnal forcings over the tropical continents, compared to the observations. The OLR time series does suggest that as α increases, the response becomes slower and less realistic. The time lag between the maximum rainfall rates and the coldest cloud tops, however, is fairly well simulated if we consider that the rainfall peak at 1900 LST in the Alpha9 run is the direct result of afternoon and early evening boundary layer heating. Another interesting feature to notice is that the rapid dissipation of mid- and high-level clouds between 0500 and 0900 LST is not well captured by the GCM. In the real world, the upper-level clouds tend to dissipate faster than lower-level clouds, as they see the sun about 10–30 min earlier. All of the simulated clouds, no matter high or low, ''see'' sunshine at the same time. Since cloud dissipation takes some time, lower-level clouds in the GCM tend to receive weaker-than-observed solar insolation and so dissipate more slowly.

Figure 9 depicts the first diurnal harmonic of the OLR from Alpha8, Alpha9, ERBE, and CERES. Observations indicate a maximum between 1000 and 1100 LST over most of the Amazon Basin, consistent with previous studies (e.g., Liebmann and Gruber 1988; Kondragunta et al. 1993). The amplitude is about 15 W m^{-2}. There are some geographical variations across the Am-

azon, in the model results. Alpha8 and Alpha9 show a maximum at about 0900 LST over the western portion of the Amazon, and a maximum between 1000 and 1100 LST over the eastern Amazon. Amplitudes over the eastern part are weaker than observed.

The most notable property of the second diurnal harmonic of the OLR (Fig. 10) is the much larger amplitude in the ERBE and CERES data than in the simulations. The ERBE and CERES data show a maximum between 2300 and 0100 LST, with an average amplitude of 5 W m^{-2}. The amplitudes in Alpha8 and Alpha9 are generally less than or close to 1 W m^{-2}. Duvel (1989) noticed that the diurnal cycle of deep convection over tropical Africa is not symmetrical, in that the period of development is usually shorter than the period of dissipation, as is also observed over the Amazon. We conclude that the second diurnal harmonic of convection is also important over the tropical continents, and should not be ignored.

c. High-cloud fraction and convective cloud types

Figure 11 shows the first diurnal harmonic of the high cloudiness from Alpha8, Alpha9, and ISCCP. ISCCP indicates a maximum at about 2200 LST. The average amplitude is about 10%–15%. Meisner and Arkin (1987), applying three temperature thresholds (220, 235, and 270 K) to infrared satellite data, examined the first diurnal harmonic in fractional cold cloudiness over the Amazon. Their analyses show that lower temperature thresholds such as 220 and 235 K tend to give a maximum at about 1800 LST, and a higher temperature threshold of 270 K gives a maximum at 0000 LST, suggesting that mid- and low-level clouds tend to peak at midnight or later, while high clouds, including deep cumuli, stratiform and anvil clouds, tend to peak at 1800 to 1900 LST, a few hours earlier. This was confirmed by Garreaud and Wallace (1997) using ISCCP data. For purposes of this study, high cloudiness is defined as clouds higher than 440 hPa (corresponding to a temperature about 255 K). The observations used here appear to be consistent with those of previous studies. Both Alpha8 and Alpha9 show a maximum between midnight and 0100 LST, about 2–3 h later than observed. The amplitudes are about 5%, weaker than observed. Again, the response of high cloudiness to diurnal deep convection in the GCM appears to be slower than observed over the tropical continents.

In the GCM, convective cloud types are classified using heights of both cloud base and cloud top. Since the clouds originating from the PBL top are dominant (Ding and Randall 1998), we show in Fig. 12 only the simulated diurnal time series of the cloud-base mass flux profile for the cumuli with their bases at the PBL top (model level 17). For example, the values at level 10 are cloud-base mass fluxes for clouds with their bases at the PBL top, and their tops at model level 10. Although the Alpha9 mass fluxes are generally smaller than those of Alpha8, both simulations give similar patterns of diurnal variations for the various convective cloud types. Almost all of the simulated cloud types, no matter how deep or shallow, have minimum cloud-base mass fluxes in the morning, and maximum cloud-base mass fluxes in the early evening between 1800 and 1900 LST. The simulated midlevel clouds are dominant, relative to the deep and shallow clouds, throughout the day. In the morning, the mid- and low-level clouds are dominant. This is different from what we expected, which is that shallow cumuli would be the dominant cloud types in the morning. However, we do not have data to prove this for the time being. After 1100 LST, all the cloud types intensify rapidly, especially deep clouds. After reaching a maximum of activity in the early evening, all of the cloud types start to dissipate. The deeper clouds appear to dissipate much faster, especially after midnight. The mid- and low-level clouds, however, redevelop somewhat after midnight, between 0100 and 0500 LST, and then dissipate again in the early morning. Overall, the model appears to predict too few shallow cumuli and too many midlevel clouds throughout the day.

d. Surface temperature and surface fluxes

Figure 13 compares the ABRACOS and simulated diurnal time series of DJF surface temperature, surface net shortwave (SW), and surface net longwave (LW) fluxes over the Amazon. The average measurement height for the three forest stations is about 50 m above the ground. The average height of the canopy top is between 30 and 40 m. Therefore, the observed ''surface'' variables are neither near-ground nor canopy quantities. This fact should be kept in mind when we compare the observations to simulated quantities.

The simulated canopy temperature is compared with the observed surface temperature. Station observations over the Amazon indicate that the surface temperature reaches its minimum (22.5°C) between 0500 and 0600 LST, and peaks in the early afternoon (28°C), around 1400 LST (Fig. 13a). The diurnal range is about 5.5 K. Alpha8 tends to put its temperature minimum (21.5°C) at about 0700 LST, and an afternoon maximum (29°C) at 1400 LST. The morning minimum is colder than observed, while the afternoon maximum is warmer than observed. The morning minimum appears to have a 1-h lag relative to observations, and the diurnal range of temperature is 2 K larger. The surface temperature from Alpha9 has a phase similar to that of Alpha8, but the 24-h average surface temperature is slightly colder. Variations of α do not appear to have a significant impact on the simulated temperature diurnal range.

Both observed and simulated DJF net surface SW over the Amazon (Fig. 13b) indicate a maximum near local solar noon. The simulated fluxes from Alpha8 and Alpha9 are very similar, and exceed the observations by about 30 W m^{-2}. The observed net surface LW flux

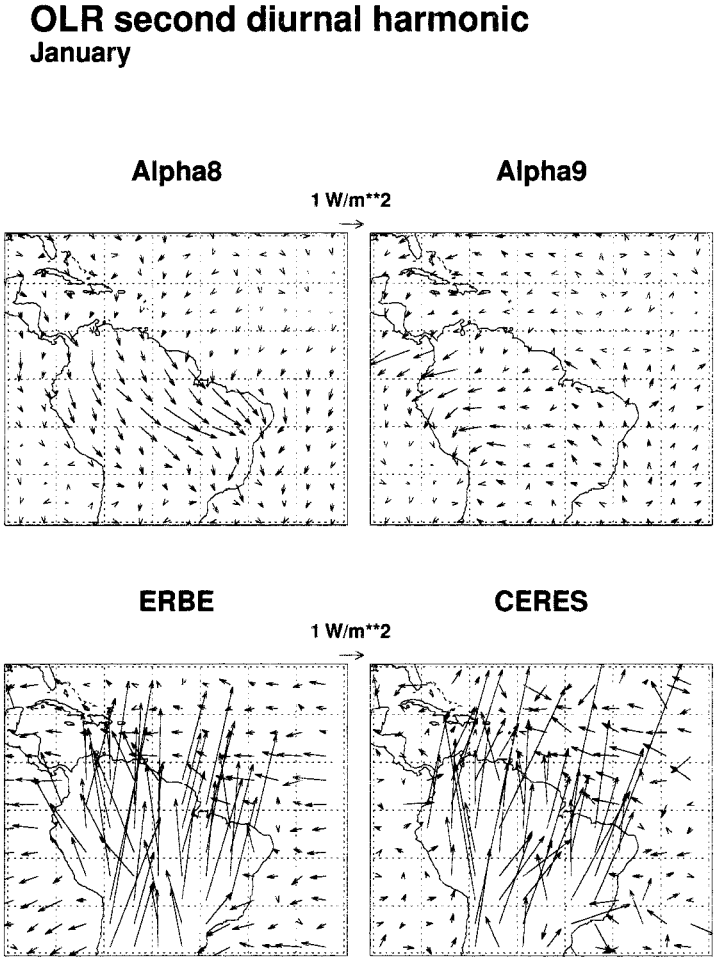

FIG. 10. Observed and simulated second diurnal harmonic of Jan OLR from Alpha8, Alpha9, and ERBE and CERES data.

(Fig. 13c) shows a minimum before sunrise at 0500 LST and a maximum at 1200 LST. The simulated LW fluxes show a minimum between 2100 and 2200 LST, and a maximum at 1300 LST. They are less than observed during the day between 0700 and 1600 LST, by an average of 15–20 W m^{-2}. Again, varying α does not strongly affect the surface net SW and LW fluxes.

It is unfortunate that ABRACOS did not provide observations of latent and sensible heat fluxes during the Southern Hemisphere summer. In Fig. 14, we compare only the simulated DJF latent and sensible heat fluxes over the Amazon. Alpha8 and Alpha9 indicate that, as expected both latent and sensible heat fluxes closely follow the local solar radiation. They remain nearly constant around 33 and -29 W m^{-2} during the night, with peaks around 350 and 90 W m^{-2} at local solar noon. The differences between Alpha8 and Alpha9 occur mainly during the day and are greatest at noon. The latent heat flux obtained in Alpha8 exceeds that of Alpha9 by 20 W m^{-2} at 1200 LST, while the sensible heat flux from Alpha8 is less than that from Alpha9 by 16 W m^{-2}.

6. Discussion and an experiment with a variable, α

The results presented above show that a single value of α is unsatisfactory. If a large value of α is used for all cloud types, the monthly mean state is realistic, but the diurnal cycle is not. If a small value of α is used, the diurnal cycle is more realistic, but the monthly mean state is less so. Our results therefore motivate us to test a simple and incomplete parameterization of the variations of α with cloud type.

Such a parameterization can be based on the work of Pan and Randall (1998), who showed that α can be expressed as

$$\alpha = \frac{1}{2\varepsilon\sigma}\int_{z_B}^{z_T}\frac{\eta^2}{\rho}\,dz. \tag{2}$$

Here ε is the fraction of the total CKE that is associated

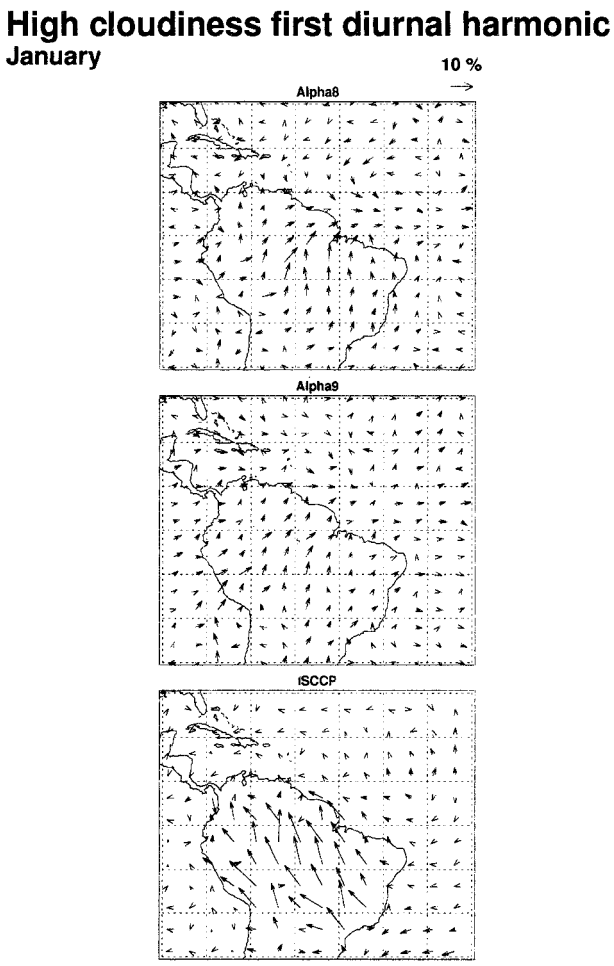

FIG. 11. Observed and simulated first diurnal harmonic of Jan high cloudiness from Alpha8, Alpha9, and ISCCP data.

with the vertical component of the convective velocity field; as shown by Xu and Arakawa (1992), smaller values of ε and larger values of α occur when the mean horizontal wind is strongly sheared in the vertical. The fractional area covered by cumulus updrafts is denoted by σ; as the strength of convective activity increases, σ is expected to increase for a given cloud-top height, corresponding to more convective clouds per unit area; according to (2), this will tend to decrease α. The normalized convective mass flux (i.e., normalized by the cloud-base value; see Arakawa–Schubert) is denoted by η. The heights of the cloud top and cloud base of the convective circulation are denoted by z_T and z_B, respectively. Finally, ρ represents the density of the air. Inspection suggests that the integral in (2) is typically an increasing function of cloud depth.

In summary, (2) shows that α depends on cloud depth, shear, and convective intensity. The effects of cloud depth, which enter through the vertical integral in (2), can be easily included for each cloud type. In order to use (2) to parameterize α, however, we also need to specify ε and σ. At present we have no established way to do this. For simplicity, therefore, we assign constant values to the shear parameter ($\varepsilon = 0.02$), and the convective fractional area ($\sigma = 0.01$), based on cloud ensemble model output of Xu (1991) and observationally based estimates by Houze (1982). We evaluate the integral in (2) using the predicted normalized mass flux profile, density sounding, and cloud-base and cloud-top levels. In this way we obtain a partial parameterization of the variability of α.

Figure 15 shows a scatterplot of the simulated values of α for cumuli with their cloud base at the PBL top and their cloud tops at various model levels; these are representative values based on detailed output in a short simulation. The values of α range from 10^6 m^4 kg^{-1} for the shallowest cumuli (with their tops at level 16) to more than 10^8 m^4 kg^{-1} for the deepest cumuli (with their tops at level 3). The mean value of α is close to 10^8 m^4 kg^{-1}. As expected, there is a general trend for the deeper (shallower) clouds to have larger (smaller) values of α. Recall that larger values of α correspond to longer adjustment times. The results shown in Fig. 15 therefore suggest that deeper (shallower) clouds are typically characterized by longer (shorter) adjustment times.

Diurnal time series of total rain rates from this variable-α run, as well as from Alpha8, are shown in Fig. 16 (each of these cases is an ensemble of two 3-month DJF runs). Although the mean values of α are close to 10^8 m^4 kg^{-1}, and the precipitation maxima still occur at 1800 LST, the diurnal range is better simulated in the variable-α run, and the peak value (about 12 mm day^{-1}) is similar to that observed. These very preliminary results encourage us to think that we can devise a parameterization of α that will permit simultaneous realistic simulations of both the monthly mean state and the diurnal cycle.

7. Summary and conclusions

Based on satellite and surface observations over the Amazon Basin, we have constructed a descriptive model of the diurnal variation of convection over tropical land area (Fig. 17). This model can be further improved by the use of TRMM and LBA observations, and can be used to compare with GCM-simulated diurnal variability. Both surface net SW and LW fluxes over the Amazon tend to follow the daytime solar insolation and peak around local noon. Surface temperature usually reaches a minimum slightly after sunrise (0600 LST) and peaks at about 1400 LST. There are always some clouds existing over the Amazon throughout the day during summer. However, they have dramatic diurnal variations in terms of cloud depth and the vigor of convection, which may significantly affect precipitation, surface sensible and latent heat fluxes. Relatively speaking, scattered, shallow clouds dominate in the morning between 0900 and 1100 LST. The rainfall rate has a

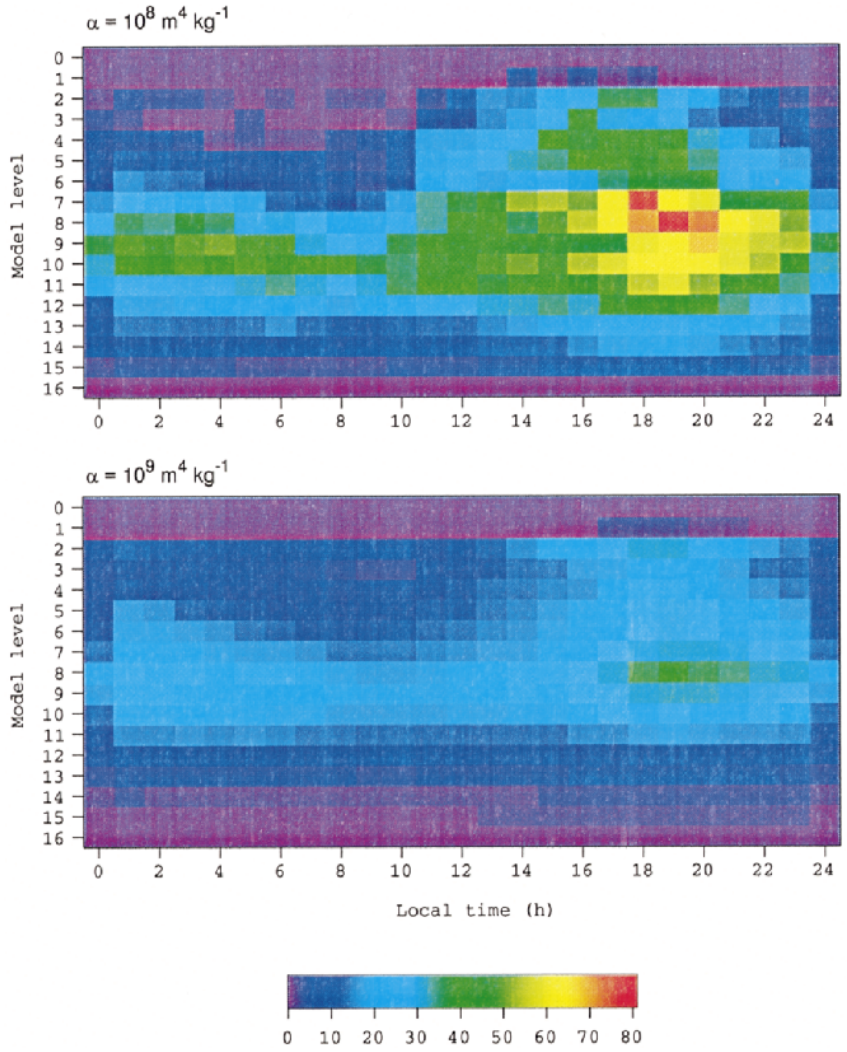

FIG. 12. Composite diurnal variation of the detrainment mass flux as a function of cloud-top level for clouds with their bases at the PBL top. The upper panel is for $\alpha = 10^8$ m^4 kg^{-1}, and the lower panel is for $\alpha = 10^9$ m^4 kg^{-1}.

minimum, while OLR reaches a maximum during this period. Responding to rapidly increasing surface temperature, all types of clouds, especially mid- and high-level clouds, gradually develop and extend to larger areas. The heaviest precipitation, mostly from deep convective clouds, occurs in the afternoon between 1500 and 1600 LST, about 1–2 h after the maximum surface temperature. Rain rates start to decrease after 1600 LST, but stratiform and anvil clouds continue to grow, and the OLR reaches a minimum at 1800 LST. The time lag between the heaviest precipitation and the coldest cloud top is about 2–3 h. Between late night and early morning, the OLR increases only slightly, largely because the stratiform and anvil clouds dissipate very slowly. Due to strong radiative cooling at cloud top, some stratiform clouds may even redevelop and form a broad, but minor, second rainfall peak between 0100 and 0400 LST. This is suggested by PR data. From 0500 to 0900 LST, the surface forcing is relatively weak, and as the sun comes out, the strong cloud-top radiative cooling quickly disappears, mid- and high-level clouds dissipate rapidly, and scattered shallow cumuli dominate.

Comparisons of simulations and observations on seasonal-mean timescales indicate that use of a larger value of α, for all cloud types, tends to produce a more realistic dynamic and thermodynamic structure of the tropical troposphere. However, the simulated TOA radiative fluxes, LW and SW cloud radiative forcings, and albedo tend to become less realistic. Since successful simulation of the diurnal variations of convection represents an important test of a model's formulation, we have compared the observed and simulated diurnal variability of the hydrologic cycle and radiative fluxes.

The use of a constant value of α, for all convective cloud types, can capture many aspects of the observed diurnal variation of convection over tropical summer

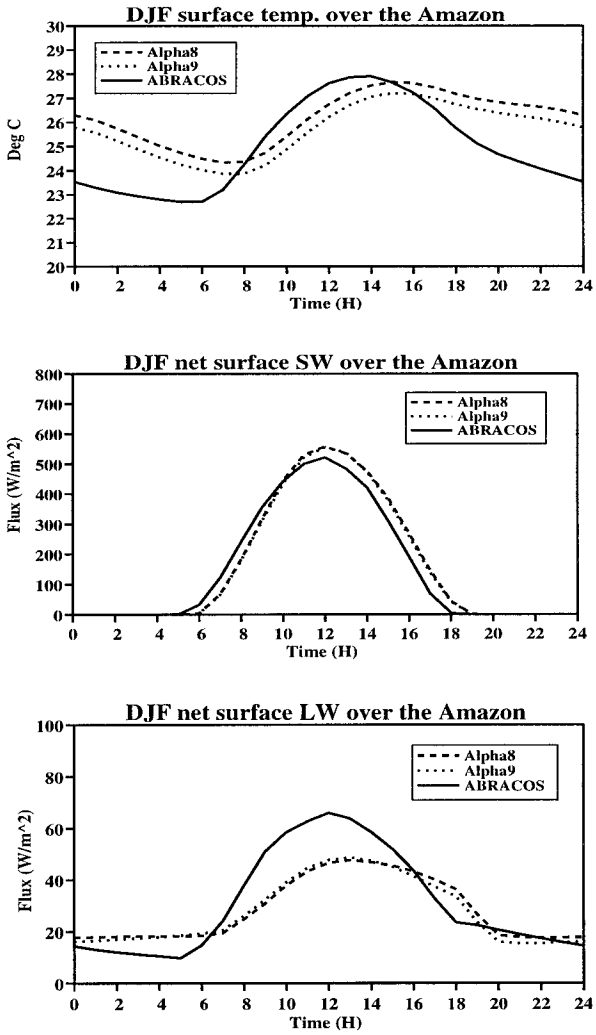

FIG. 13. Observed and simulated diurnal time series of DJF surface temperature (°C), surface net shortwave, and surface net longwave fluxes (W m^{-2}) over the Amazon.

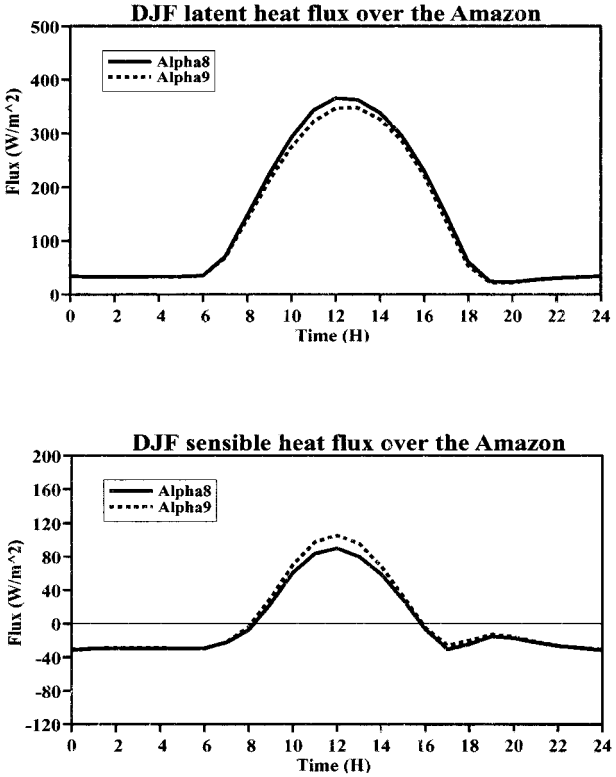

FIG. 14. Simulated diurnal time series of DJF surface sensible and latent heat fluxes (W m^{-2}) over the Amazon.

continents, especially in the Alpha8 run. However, there are some important limitations.

1) Although the simulated convective rainfall rate correctly shows a minimum between 0900 and 1000 LST, the maximum tends to lag observations by a few hours. As α increases, the convective rain rate lags the observation more, and its diurnal range becomes unrealistically small, indicating that the simulated afternoon convection over tropical summer continents develops much too slowly in response to daytime surface heating. This we interpret as a consequence of the longer adjustment times associated with larger values of α.
2) The stratiform cloud parameterization tends to give a rainfall peak in the early morning, similar to observations. Although the peak stratiform rainfall rate also lags the observation by 2–3 h, this probably stems from the lag in peak convective rainfall. As α increases, convective precipitation decreases, and stratiform precipitation undergoes a nearly compensating increase. The unrealistically strong stratiform precipitation (and unrealistically weak convective precipitation) interfere with the simulation of the diurnal variation of the hydrologic cycle and tend to shift the commonly observed afternoon total rainfall peak to early morning.
3) Although the time lag between the heaviest precipitation and the coldest cloud top is well captured by the GCM, the OLR time series and high-cloudiness data also suggest that the larger α is the slower the response. This is the reason why the second diurnal harmonics are quite large in observations, but much weaker in GCM simulations.
4) Although increasing α changes the ratio of simulated tropical convective and stratiform precipitation, it does not appear to have a strong impact on the simulated surface sensible and latent heat fluxes.

In summary, a larger value of α tends to produce a less realistic diurnal variation of the hydrologic cycle and radiative fluxes. As shown by Randall and Pan (1993), larger values of α correspond to longer adjustment times. We hypothesize that the large value of α is realistic for the deeper clouds and so favorably

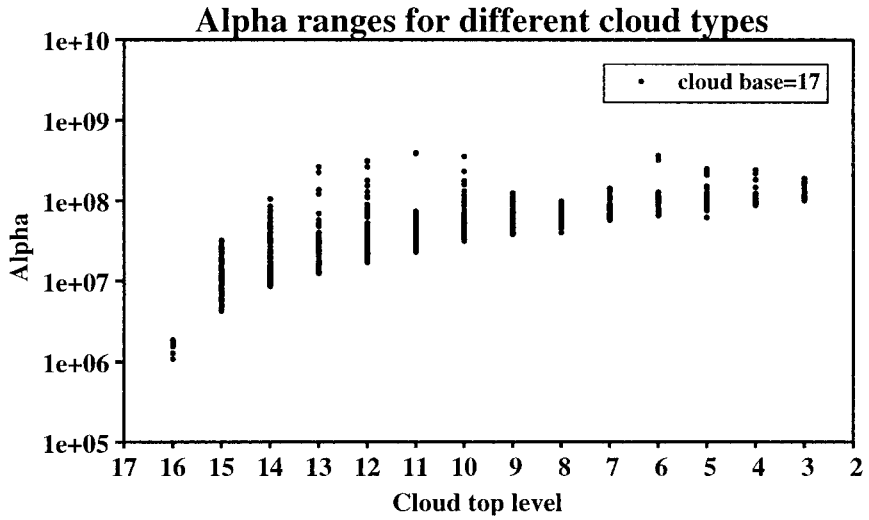

FIG. 15. Ranges of α (m^4 kg^{-1}) for clouds with cloud base at level 17.

impacts their interactions with the large-scale circulation, while the same large value of α is unrealistic for the shallower clouds and so interferes with the simulated diurnal cycle and radiative fluxes. We conclude that the use of a single constant value to α for all cloud types is an unacceptably crude idealization. A theory to determine α will lead to improved realism of the simulated diurnal cycle. Preliminary tests of a parameterization that permits α to vary in a simplified way have produced some improvement in the simulated diurnal variability of convection.

Acknowledgments. The TRMM TMI and PR data were provided by the NASA Goddard Space Flight Center Data Archive and Distribution Center. Many thanks to Drs. Chris Kummerow, Hong Ye, and Song Yang for help with the TRMM data. The ERBE, CERES, and ISCCP data were provided by the NASA Langley Atmospheric Science Data Center. The ABRACOS surface data were made available by the U.K. Institute of Hydrology and the Instituto Nacional de Pesquisas Espaciais (Brazil). Professor Steve Rutledge, Drs. Todd Ringler and Kuanman Xu made helpful comments and suggestions in the early version of the paper. Special thanks for two anonymous reviewers for critical and constructive comments that greatly improved the paper. This research has been supported by NASA, Grants NAG5-4749 and NAS1-98125 from Colorado State University

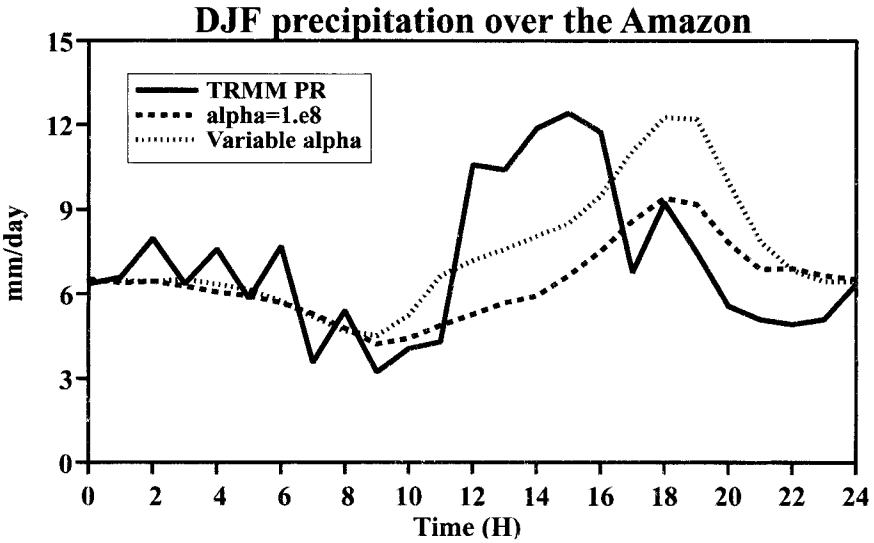

FIG. 16. Diurnal time series of Jan total precipitation for Alpha8 and a variable-α run.

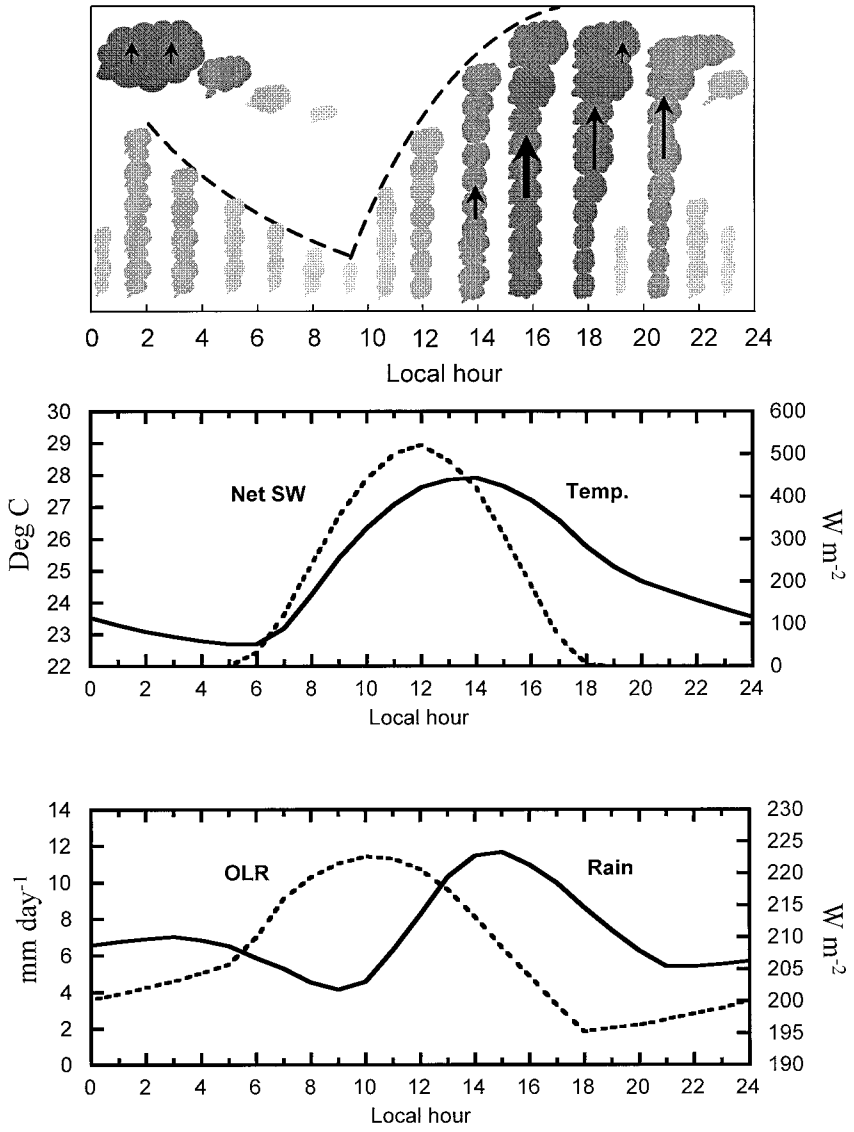

FIG. 17. A descriptive model showing the diurnal variation of convection over tropical summer continents.

and Grant ATM-9812384 from the National Science Foundation.

REFERENCES

Barkstrom, B. R., 1984: The Earth Radiation Budget Experiment (ERBE). *Bull. Amer. Meteor. Soc.,* **65,** 1170–1185.

Bergman, J. W., and M. L. Salby, 1996: Diurnal variations of cloud cover and their relationship to climatological conditions. *J. Climate,* **9,** 2802–2820.

——, and ——, 1997: The role of cloud diurnal variations in the time-mean energy budget. *J. Climate,* **10,** 1114–1124.

Brooks, D. R., and P. Minnis, 1984: Comparison of longwave diurnal models applied to simulation of the Earth Radiation Budget Experiment. *J. Climate Appl. Meteor.,* **23,** 155–160.

Chen, M., R. E. Dickinson, X. Zeng, and A. N. Hahmann, 1996: Comparisons of precipitation observed over the continental United States to that simulated by a climate model. *J. Climate,* **9,** 2233–2249.

Dai, A., K. E. Trenberth, and T. R. Karl, 1999a: Effects of clouds, soil moisture, precipitation, and water vapor on diurnal temperature range. *J. Climate,* **12,** 2451–2473.

——, F. Giorgi, and K. E. Trenberth, 1999b: Observed and model-simulated diurnal cycles of precipitation over the contiguous United States. *J. Geophys. Res.,* **104,** 6377–6402.

Ding, P., and D. A. Randall, 1998: A cumulus parameterization with multiple cloud base levels. *J. Geophys. Res.,* **103,** 11 341–11 353.

Duvel, J. P., 1989: Convection over tropical Africa and the Atlantic Ocean during northern summer. Part I: Interannual and diurnal variations. *Mon. Wea. Rev.,* **117,** 2782–2799.

Eitzen, Z. A., and D. A. Randall, 1999: Sensitivity of the simulated Asian summer monsoon to parameterized physical processes. *J. Geophys. Res.,* **104,** 12 177–12 191.

Fowler, L. D., D. A. Randall, and S. A. Rutledge, 1996: Liquid and ice cloud microphysics in the CSU general circulation model.

Part I: Model description and simulated microphysical processes. *J. Climate,* **9,** 489–529.

Garreaud, R. D., and J. M. Wallace, 1997: The diurnal march of convective cloudiness over the Americas. *Mon. Wea. Rev.,* **125,** 3157–3171.

Gates, W. L., 1992: AMIP: The Atmospheric Model Intercomparison Project. *Bull. Amer. Meteor. Soc.,* **73,** 1962–1970.

Gray, W. M., and R. W. Jacobson, 1977: Diurnal variation of deep cumulus convection. *Mon. Wea. Rev.,* **105,** 1171–1188.

Harrison, E. F., D. R. Brooks, P. Minnis, B. A. Wielicki, W. F. Staylor, G. G. Gibson, D. F. Young, F. M. Denn, and the ERBE Science Team, 1988: First estimates of the diurnal variation of longwave radiation from multiple-satellite Earth Radiation Budget Experiment (ERBE). *Bull. Amer. Meteor. Soc.,* **69,** 1144–1151.

Hartmann, D. L., K. Kowalewsky, and M. L. Michelsen, 1991: Diurnal variations of outgoing longwave radiation and albedo from ERBE scanner data. *J. Climate,* **4,** 598–617.

Hendon, H. H., and K. Woodberry, 1993: The diurnal cycle of tropical convection. *J. Geophys. Res.,* **98,** 16 623–16 637.

Houze, R. A., Jr., 1982: Cloud clusters and large-scale vertical motions in the tropics. *J. Meteor. Soc. Japan,* **60,** 396–410.

——, 1989: Observed structure of mesoscale convective systems and implications for large-scale heating. *Quart. J. Roy. Meteor. Soc.,* **115,** 425–461.

——, 1997: Stratiform precipitation in regions of convection: A meteorological paradox? *Bull. Amer. Meteor. Soc.,* **78,** 2179–2196.

Huffman, G. J., and Coauthors, 1997: The Global Precipitation Climatology Project (GPCP) combined precipitation dataset. *Bull. Amer. Meteor. Soc.,* **78,** 5–20.

Karl, T. R., and P. M. Steurer, 1990: Increased cloudiness in the United States during the first half of the twentieth century: Fact or fiction? *Geophys. Res. Lett.,* **17,** 1925–1928.

——, and Coauthors, 1993: Asymmetric trends of daily maximum and minimum temperature. *Bull. Amer. Meteor. Soc.,* **74,** 1007–1023.

Kondragunta, C. R., H. L. Kyle, and A. T. Mecherikunnel, 1993: Diurnal variation of the outgoing long-wave radiation: As revealed by the E.R.B.E. *Tellus,* **45A,** 1–14.

Kousky, V. E., 1980: Diurnal rainfall variation in northeast Brazil. *Mon. Wea. Rev.,* **108,** 488–498.

Kummerow, C., W. Barnes, T. Kozu, J. Shiue, and J. Simpson, 1998: The Tropical Rainfall Measuring Mission (TRMM) sensor package. *J. Atmos. Oceanic Technol.,* **15,** 809–817.

Liebmann, B., and A. Gruber, 1988: The annual variation of the diurnal cycle of outgoing longwave radiation. *Mon. Wea. Rev.,* **116,** 1659–1670.

——, J. A. Marengo, J. D. Glick, V. E. Kousky, I. C. Wainer, and O. Massambani, 1998: A comparison of rainfall, outgoing longwave radiation, and divergence over the Amazon Basin. *J. Climate,* **11,** 2898–2909.

Meisner, B. N., and P. A. Arkin, 1987: Spatial and annual variations in the diurnal cycle of large-scale tropical convective cloudiness and precipitation. *Mon. Wea. Rev.,* **115,** 2009–2032.

Minnis, P., and E. Harrison, 1984: Diurnal variability of regional cloud and clear-sky radiative parameters derived from GOES data. Part II: November 1978 cloud distributions. *J. Climate Appl. Meteor.,* **23,** 1012–1031.

Pan, D.-M., and D. A. Randall, 1998: A cumulus parameterization with a prognostic closure. *Quart. J. Roy. Meteor. Soc.,* **124,** 949–981.

Randall, D. A., and D.-M. Pan, 1993: Implementation of the Arakawa–Schubert cumulus parameterization with a prognostic closure. *The Representation of Cumulus Convection in Numerical Models, Meteor. Monogr.,* No. 46, 137–144.

——, Harshvardhan, and D. A. Dazlich, 1991: Diurnal variability of the hydrologic cycle in a general circulation model. *J. Atmos. Sci.,* **48,** 40–62.

Rossow, W. B., and R. A. Schiffer, 1991: ISCCP cloud data products. *Bull. Amer. Meteor. Soc.,* **72,** 2–20.

Rutledge, S. A., and R. A. Houze Jr., 1987: A diagnostic modeling study of the trailing stratiform region of a midlatitude squall line. *J. Atmos. Sci.,* **44,** 2640–2656.

Sellers, P. J., D. A. Randall, G. J. Collatz, J. Berry, C. Field, D. A. Dazlich, C. Zhang, and L. Bounoua, 1996a: A revised land surface parameterization (SiB2) for atmospheric GCMs. Part I: Model formulation. *J. Climate,* **9,** 676–705.

——, S. O. Los, C. J. Tucker, C. O. Justice, D. A. Dazlich, G. J. Collatz, and D. A. Randall, 1996b: A revised land surface parameterization (SiB2) for atmospheric GCMs. Part II: The generation of global fields of terrestrial parameters from satellite data. *J. Climate,* **9,** 706–737.

Short, D. A., and J. M. Wallace, 1980: Satellite-inferred morning-to-evening cloudiness changes. *Mon. Wea. Rev.,* **108,** 1160–1168.

Shuttleworth, W. J., J. H. C. Gash, J. M. Roberts, C. A. Nobre, L. C. B. Molion, and N. M. G. Ribeiro, 1991: Post-deforestation Amazonian climate: Anglo-Brazilian research to improve prediction. *J. Hydrol.,* **129,** 71–86.

Silva Dias, P. L., J. P. Bonatti, and V. E. Kousky, 1987: Diurnally forced tropical tropospheric circulation over South America. *Mon. Wea. Rev.,* **115,** 1465–1478.

Simpson, J., R. F. Adler, and G. R. North, 1988: Proposed tropical rainfall measuring mission (TRMM) satellite. *Bull. Amer. Meteor. Soc.,* **69,** 278–295.

Slingo, A., R. C. Wilderspin, and S. J. Brentnall, 1987: Simulation of the diurnal cycle of outgoing longwave radiation with an atmospheric GCM. *Mon. Wea. Rev.,* **115,** 1451–1457.

Wallace, J. M., 1975: Diurnal variations in precipitation and thunderstorm frequency over the conterminous United States. *Mon. Wea. Rev.,* **103,** 406–419.

Wielicki, B. A., and B. R. Barkstrom, 1991: Clouds and the Earth's Radiant Energy System (CERES): An earth observing system experiment. Preprints, *Second Symp. on Global Climate Change Studies,* New Orleans, LA, Amer. Meteor. Soc., 11–16.

Xie, P., and P. A. Arkin, 1996: Analyses of global monthly precipitation using gauge observations, satellite estimates, and numerical model predictions. *J. Climate,* **9,** 840–858.

Xu, K.-M., 1991: The coupling of cumulus convection with large-scale processes. Ph.D. dissertation, Department of Atmospheric Science, University of California, Los Angeles, Los Angeles, CA, 250 pp. [Available from Department of Atmospheric Science, University of California, Los Angeles, Los Angeles, CA 90024.]

——, and A. Arakawa, 1992: Semiprognostic tests of the Arakawa–Schubert cumulus parameterization using simulated data. *J. Atmos. Sci.,* **49,** 2421–2436.